

## EXTENSION OF REFRACTORINESS IN A MODEL OF CARDIAC DEFIBRILLATION

N. A. TRAYANOVA, F. AGUEL

*Department of Biomedical Engineering, Tulane University, New Orleans, LA 70118*

K. SKOUBINE

*Department of Mathematics, Tulane University, New Orleans, LA 70118, USA*

This simulation study presents an inquiry into the mechanisms by which a strong electric shock halts life-threatening cardiac arrhythmias. It examines the “extension of refractoriness” hypothesis for defibrillation which postulates that the shock induces an extension of the refractory period of cardiac cells thus blocking propagating waves of arrhythmia and fibrillation. The present study uses a model of the defibrillation process that represents a sheet of myocardium as a bidomain with unequal anisotropy ratios. The tissue consists of curved fibers in which spiral wave reentry is initiated. The defibrillation shock is delivered via two line electrodes that occupy opposite tissue boundaries. Simulation results demonstrate that a large-scale region of depolarization is induced throughout most of the tissue. This depolarization extends the refractoriness of the cells in the region. In addition, new wavefronts are generated from the regions of induced hyperpolarization that further restrict the spiral wave pathway and cause its termination.

### 1 Introduction

Current understanding of the mechanism for cardiac defibrillation considers prevention of wavefront propagation by the shock to be central for defibrillation. A large body of research has confirmed that the shock extends the refractoriness of tissue traversed by fibrillatory pathways<sup>1,2,3,4</sup> and thus, the wavefronts die out since they have nowhere to go. Currently, extension of refractoriness by the shock is attributed to the production of the so-called *graded response*<sup>3,5,6,7</sup> which constitutes an extension of action potential duration (APD) of each cell in the myocardium, and is initiated by a large shock-induced membrane depolarization. Clearly, this concept implies that every cell affected by the shock undergoes some level of membrane depolarization.

However, recent measurements<sup>8,9,10</sup> and computer simulations<sup>11,12</sup> revealed that the spatial distribution of transmembrane potential induced by the defibrillation shock is more complex than previously expected. These studies have demonstrated that the membrane is hyper- or depolarized throughout regions that comprise many cardiac cells (these regions are termed “virtual electrodes”). This evidence seems to conflict with the understanding of the contribution of the extension of refractoriness in the defibrillation process.

The goal of this simulation research is to examine the contribution of the extension of cellular refractoriness to defibrillation in a tissue model that permits the formation of virtual electrodes during the shock. To better understand the results of our tissue-level simulation results, we initially examine the effect of shock-induced depolarization and hyperpolarization on the refractoriness of a single isolated cell. Then, we proceed to examine refractoriness following the shock in the two-dimensional tissue model that consists of interconnected cells forming curved fibers. The tissue is represented as a bidomain of unequal anisotropy ratios, thus permitting extracellular intervention with a defibrillation shock. We simulate arrhythmia by inducing a spiral wave reentry and extinguish it by a defibrillation shock delivered via two parallel extracellular electrodes. We demonstrate that the success of the shock depends on the extension of refractoriness at the virtual cathode as well as on the ability of the shock to generate new wavefronts at the border between depolarized and hyperpolarized regions in the myocardium.

## 2 Methods

To describe the membrane kinetics of cardiac tissue, we employ the modified version of the Beeler-Reuter model<sup>13</sup>, namely the BRDR membrane kinetics equations<sup>14</sup>. However, these equations need to be further modified before we can experiment with high-strength shocks. The rationale for this is that ionic models of active tissue are originally derived from voltage-clamp experiments, which provide data mostly for the voltage range of a normal action potential. When the transmembrane potential,  $V_m$ , exceeds the limits of this range due to a strong depolarization or hyperpolarization, namely  $V_m > 100 \text{ mV}$  and  $V_m < -85 \text{ mV}$  for the BRDR model, the equations become unstable and lead to non-physiological results. Thus, to conduct simulation research in defibrillation, we modified the BRDR model equations ensuring their stability for high-energy shocks. The modification used here is described in a previous publication of ours<sup>15</sup>. Further, to account for the fact that APD in a fibrillating ventricle is considerably shorter than a normal action potential, we decrease the APD of a single cell to approximately  $100 \text{ msec}$ <sup>15</sup>. It is this final version of the action potential kinetics that is used to examine the effect of depolarizing and hyperpolarizing shocks on both single cells and myocardial sheets.

To study the collective behavior of cells in intact cardiac tissue during and after the defibrillation shock, we use the bidomain model of cardiac tissue (for a review of the bidomain model refer to<sup>16</sup>). The following coupled differential equations are employed:

$$\nabla \cdot (\hat{\sigma}_i \nabla \Phi_i) = i_m, \quad \text{in } \Omega, \quad (1)$$

$$\nabla \cdot (\hat{\sigma}_e \nabla \Phi_e) = -i_m, \quad \text{in } \Omega, \quad (2)$$

$$i_m = \beta \left( C_m \frac{\partial V_m}{\partial t} + I_{ion}(V_m) - I_{stim}(t) + G(V_m, t) V_m \right), \quad \text{in } \Omega, \quad (3)$$

where  $\hat{\sigma}_i$  ( $mS/cm$ ) and  $\hat{\sigma}_e$  are conductivity tensors in the intra- and extracellular domains, respectively,  $i_m$  ( $\mu A/cm^3$ ) is the volume density of the transmembrane current,  $\beta$  ( $cm^{-1}$ ) is the surface-to-volume ratio of the tissue,  $C_m$  ( $\mu F/cm^2$ ) is the specific membrane capacitance,  $I_{stim}$  ( $\mu A/cm^2$ ) represents the transmembrane stimulation current density, and  $G$  ( $mS/cm^2$ ) is the variable membrane conductance that incorporates membrane electroporation<sup>15,17</sup>.

In the tissue model, the homogeneous Neumann boundary conditions are used representing the fact that the preparation is surrounded by an insulator,

$$\vec{n} \cdot (\hat{\sigma}_i \nabla \Phi_i) = 0, \quad \vec{n} \cdot (\hat{\sigma}_e \nabla \Phi_e) = 0, \quad \text{on } \partial\Omega, \quad (4)$$

where  $\Omega$  is the square tissue domain of dimensions 2 by 2  $cm$ .

To account for change in fiber orientation in the myocardium, we assume that cells in the sheet form curved pathways. We choose parabolic fibers since they are characterized with non-uniform fiber curvature along a fiber pathway. In a model tissue preparation with changing fiber orientation, although the intrinsic longitudinal and transverse conductivities of a fiber (and its associated extracellular space) remain constant as the fiber bends, the global conductivities (with respect to a fixed coordinate system) in the tissue change from point to point. It is the latter conductivities that participate in the equations above. In a two-dimensional preparation, the relationship between the global tissue conductivities and the ones intrinsic to a fiber is given by the following expressions:

$$\hat{\sigma}_i \equiv \begin{pmatrix} \sigma_{xx}^i & \sigma_{xy}^i \\ \sigma_{yx}^i & \sigma_{yy}^i \end{pmatrix} = \hat{R} \cdot \begin{pmatrix} \sigma_l^i & 0 \\ 0 & \sigma_t^i \end{pmatrix} \cdot \hat{R}^{-1}, \quad (5)$$

$$\hat{\sigma}_e \equiv \begin{pmatrix} \sigma_{xx}^e & \sigma_{xy}^e \\ \sigma_{yx}^e & \sigma_{yy}^e \end{pmatrix} = \hat{R} \cdot \begin{pmatrix} \sigma_l^e & 0 \\ 0 & \sigma_t^e \end{pmatrix} \cdot \hat{R}^{-1} \quad (6)$$

where  $\hat{R}$  is a matrix reflecting the local change in fiber orientation, and  $\hat{R}^{-1}$  is its inverse.  $\sigma_l^i$ ,  $\sigma_t^i$ ,  $\sigma_l^e$  and  $\sigma_t^e$  denote the intrinsic longitudinal (subscript  $l$ ) and transverse (subscript  $t$ ) bidomain conductivities of a fiber. The values of the latter used here are the same as in a paper by Roth<sup>18</sup>.

To simulate arrhythmic behavior in the sheet, we initiate a single reentrant circuit utilizing an  $S1-S2$  stimulation protocol described previously in<sup>19</sup>. The resulting reentrant wave is stable with the period of rotation 71  $msec$ . The defibrillation shock is administered through line electrodes that occupy the

entire length of opposite tissue boundaries at the top and bottom of the tissue. The shock is monophasic, of duration 10 *msec*, and of varying strength.

To solve the bidomain equations we first replace the spatial differential operators by finite differences. The ODEs are then solved using a predictor-corrector method (PECE). We employ an iterative technique, GMRES; the version used here is diagonally-preconditioned. The semi-implicit PECE method is a two-step Adams-Bashforth predictor with a two-step Adams-Moulton corrector.

### 3 Results

#### 3.1 Effects of shocks on single cells

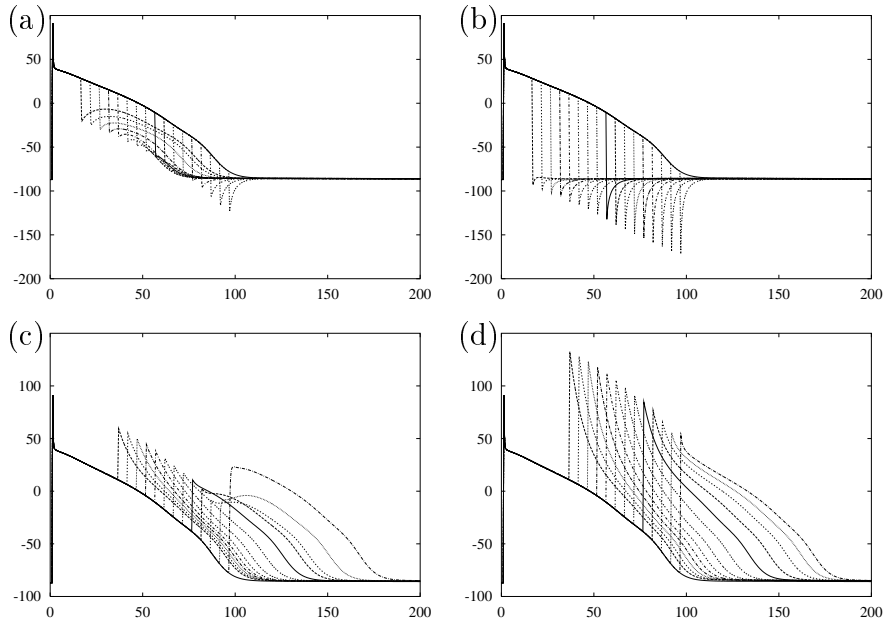


Figure 1: Response of modified BRDR membrane model to premature monophasic shocks in single cells. Horizontal axis is time (*msec*) and vertical axis is transmembrane potential (*mV*). Panels (a) and (b) show the effects of weak ( $1.5 \times$  diastolic threshold) and strong ( $3.8 \times$  diastolic threshold) hyperpolarizing shocks, respectively, for coupling intervals of 15–95 *msec*. Panels (c) and (d) show the effect of depolarizing shocks for the same strengths and coupling intervals of 35 – 95 *msec*.

Fig. 1 shows the effect of monophasic pulses applied during the refractory period of a single cell action potential. Two hyper- and two de-polarizing pulse trains for two different shock strengths are examined in the four panels of the figure. The shocks from each train are delivered at increasing coupling intervals (CIs) and the membrane responses are shown as consecutive traces on top of the original cellular action potential. The figure demonstrates that weak hyperpolarizing pulses (panel (a)) shorten the APD. The timing of the shock is very important – the earlier the shock into the cellular action potential (i.e., the shorter the CI), the less the shortening in APD. Strong hyperpolarizing pulses (panel (b)) have a similar effect on the APD, with short coupling intervals causing shorter APDs. Another difference between strong and weak hyperpolarizing pulses is that the weak pulse seems to shorten APD after its release; the action potential is actually not terminated. For a strong hyperpolarizing shock, the pulse seems to kill the action potential.

The depolarizing pulses in Fig. 1 (panels (c) and (d)) cause an extension of the APD (and thus the refractory period of the cell). Strong depolarizing shocks (panel (d)) cause an extension in APD that depends on the CI. Weak depolarizing shocks (panel (c)) elicit a response that is markedly different for different CIs. For the longest CI, the response resembles a new action potential; at the tissue level this could result in a slow-propagating action potential.

Thus, the response of cells shocked while undergoing an AP varies, depending on the shock strength as well as on the timing of the stimulus. These results of ours are consistent with some of the model findings of Jones and co-workers<sup>20,21</sup>, and Fishler *et al.*<sup>22,23</sup>. Our major contribution here is that we are able to demonstrate, for the first time, cellular responses for high-strength shocks, such as those delivered during clinical defibrillation procedures. Myocardial behavior as shown here was reported in experiments by Dillon<sup>1</sup> using potentiometric dye techniques, as well as by Tovar<sup>24</sup> using monophasic action potential recordings.

### 3.2 Extension of refractoriness in a sheet of myocardium

Fig. 2 demonstrates a spiral wave reentry and its termination by a defibrillation shock delivered by two line electrodes located at the top and bottom tissue boundaries; cathode is at the bottom, anode is at the top. The electrodes deliver a uniform electric field; the shock strength is  $6\text{ V/cm}$ . The first panel in Fig. 2 (200 ms after the onset of the spiral wave) depicts the spiral wave at the time of shock delivery; an excitable gap located near the bottom edge of the tissue is visible in this panel. Consistent with previous studies of our on virtual electrodes in tissue with curved fibers<sup>25,26,27</sup>, the shock depolarizes

the majority of the tissue, with hyperpolarization induced near the top, left, and right edges. The depolarizing stimulus falls partly over the excitable gap, directly depolarizing it. At the end (break) of the shock, new wavefronts are elicited at the upper corners as well as the bottom left corner of the tissue (frame  $t=215.0$ ). These wavefronts propagate along the borders of the tissue (frame  $t=222.0$ ) where transient hyperpolarization has decreased the threshold for excitation (this is consistent with findings in<sup>20,21,24</sup>). Eventually, all tissue is depolarized and no excitable areas remain (frame  $t=239.0$ ). The original spiral wave is extinguished thus rendering the shock “successful”.

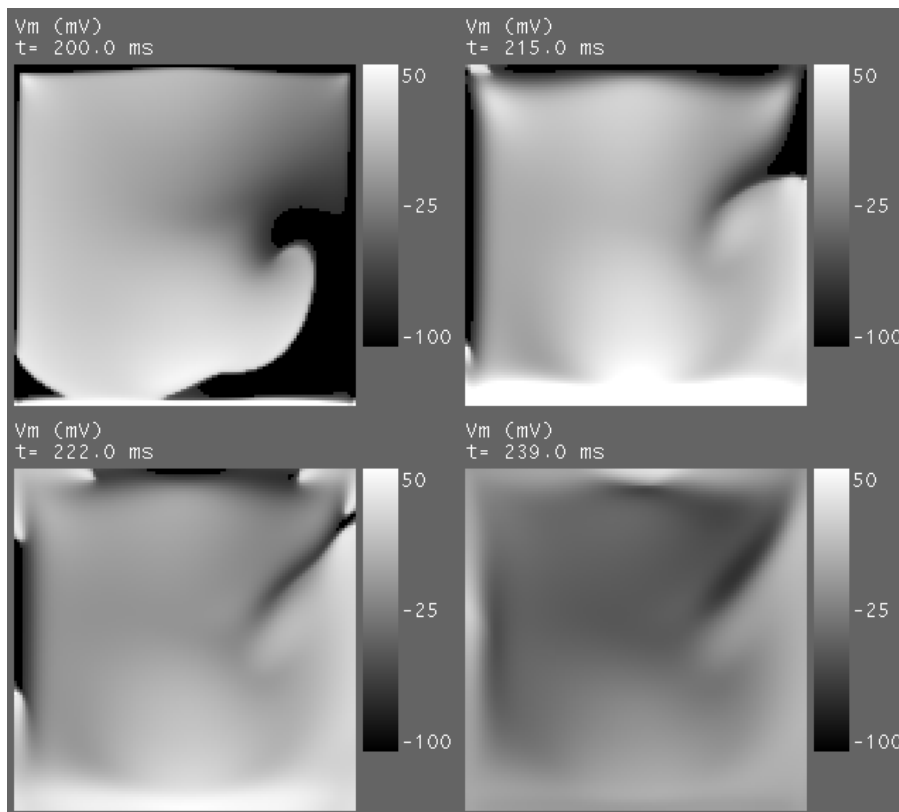


Figure 2: Selected frames from a successful defibrillation experiment. The time from the onset of spiral wave is shown in the upper left corner of each frame. The cathode is at the bottom edge, and the anode at the top edge of the tissue. Fibers are parabolic and concave down. In order to accentuate the excitable region, transmembrane potentials below 90% repolarization (-71 mV) were artificially assigned black.

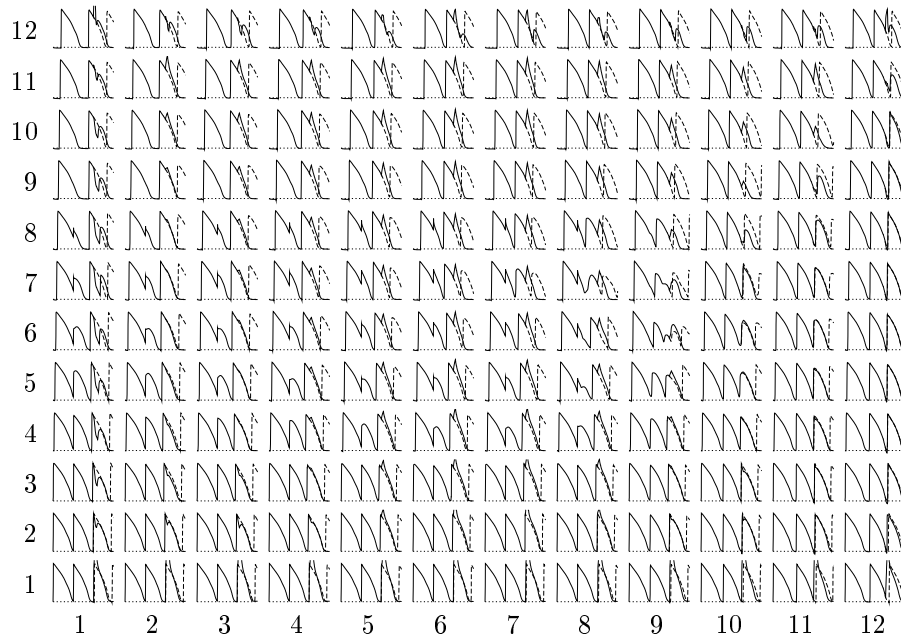


Figure 3: Time recordings of transmembrane potential at 144 locations in the tissue for the successful defibrillation shock in Fig. 2. Spacing between recording electrodes is  $1.67\text{ mm}$ . Traces at the edges are  $0.83\text{ mm}$  from the tissue border. In the text, the position of individual traces refer to the numbers shown such that trace (2,4) refers to the trace second from the left and fourth from the bottom. The resting potential ( $-84\text{ mV}$ ) is shown as a dotted line. A portion of the time course of the transmembrane potential of the undisturbed spiral wave is shown as a dashed recording. The transmembrane potential of the shocked rotor is shown as a solid trace. The range of transmembrane potential shown is  $-100$  to  $50\text{ mV}$ . The total time for all recordings is  $299\text{ msec}$ .

Fig. 3 is the “recording electrode” map for the above simulation. It displays, at locations on a regular 12 by 12 grid in the myocardial sheet, the time course of the transmembrane potential from the time before the shock until the return of the tissue to resting conditions after the shock. Superimposed over each trace is the course of the transmembrane potential associated with the spiral wave if left undisturbed. The difference in traces at each recording point constitutes the shock-induced change in transmembrane potential. Extension of refractoriness is evident in the central portion of the tissue. It is associated with the formation of the virtual cathode that occupies the majority of the myocardial mass. The extension of the refractory period in the middle region (see traces (4-8,6-6), traces (3-10,8-9) and traces (2-11,10-11), for instance)

ensures that this region does not become excitable as the wavefronts generated in the former hyperpolarized regions near the top tissue edges attempt to propagate through it. Thus the wavefronts run out of space to propagate through and ultimately die out “terminating the arrhythmia”. By the time an excitable region appears ( $t=247.0 \text{ msec}$ , not shown here) adjacent tissue is not sufficiently depolarized to cause re-excitation. Eventually all tissue returns to rest, ensuring the success of the shock.

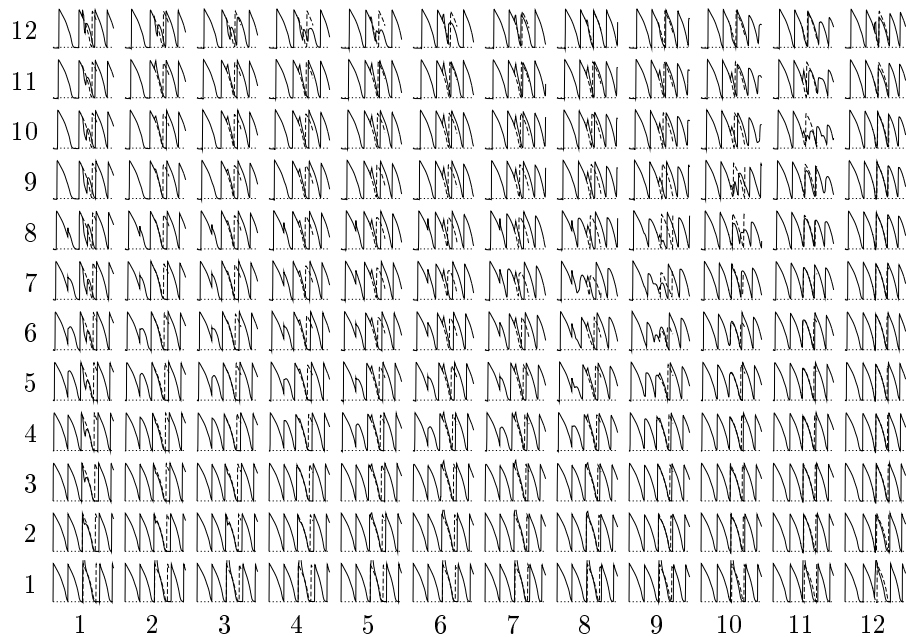


Figure 4: Time recordings of transmembrane potential at the same 144 locations as in Fig. 3 for an unsuccessful defibrillation shock experiment. The total time for all recordings is  $412 \text{ msec}$  and the transmembrane potential range is  $-100$  to  $50 \text{ mV}$ . Refer to the caption of Fig. 3 for further detail.

Fig. 4 is the “recording electrode” map and Fig. 5 is a sequence of selected frames for another simulation experiment. The only difference between this simulation and the previous is the strength of the shock, now  $4 \text{ V/cm}$ . Since this shock is weaker, no new wavefront is elicited at the top right corner of the tissue (frame  $t=220.0$ ) due to lower values of induced hyper- and depolarization there. Because the reentrant wavefront is approaching the upper right corner, this subtle difference has a significant impact on the outcome of the

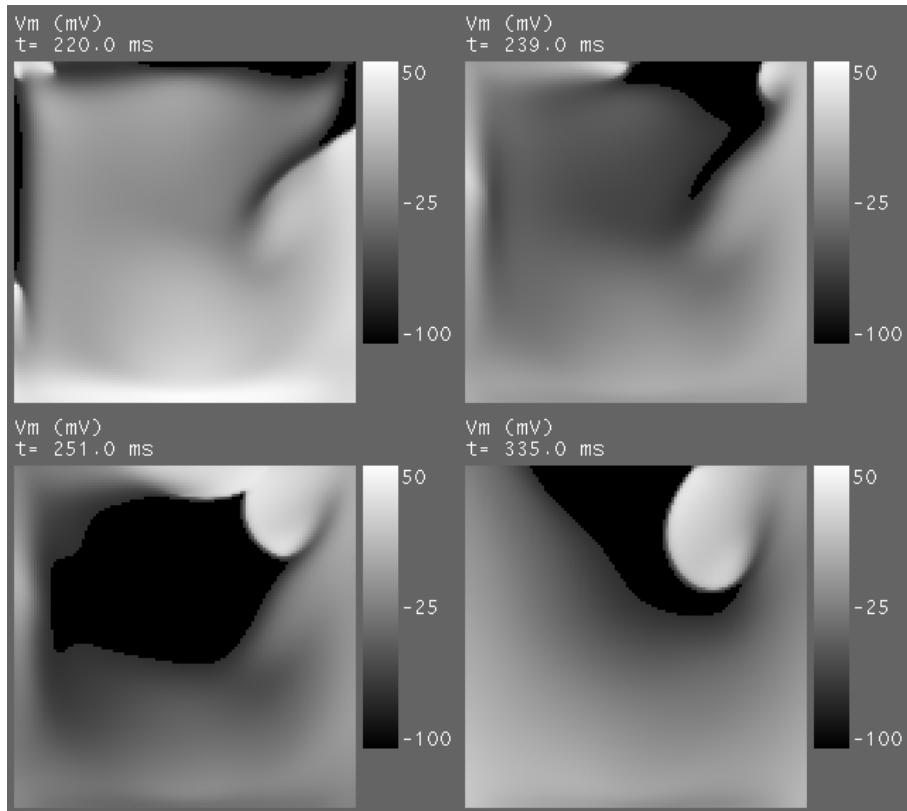


Figure 5: Selected frames from the same unsuccessful defibrillation experiment as shown in Fig. 4. The tissue and electrode geometries are the same as for the successful defibrillation shock experiment (see Fig. 2 caption).

shock. It takes longer for the excitable areas (made excitable by the transient hyperpolarization) to become depolarized. At frame  $t=239.0$  in Fig. 2, all tissue is depolarized. In Fig. 5 frame  $t=239.0$ , however, there still exists an excitable area. Furthermore, because of the lower shock intensity, tissue that was refractory at the end of the shock is now becoming excitable again. By the time the waves collide along the top border of the tissue (frame  $t=251.0$ ), there is a large excitable area ahead of the wavefront. As a result, the wave continues to propagate (frame  $t=335.0$ ). As evident from Fig. 4, the failure to extend refractoriness sufficiently compared to the case of undisturbed spiral wave (see traces (7-10,11)) allows for the continuation of the propagating wave-

front. Note in these traces that the second cycle (the first full action potential) begins just as the first cycle is reaching resting potential (the dashed line in the traces). Thus the region under those “recording electrodes” is close to being fully excitable by the time the wavefront gets there which is the ultimate reason for the failure of the shock in this simulation.

#### 4 Discussion

In this simulation study we examine the response of single cells and cardiac tissue sheets to defibrillation shocks. The purpose of the research is to study the extension of cellular refractoriness induced by the shock and its role in preventing the propagation of the wavefronts of arrhythmia and fibrillation.

Previous research<sup>1,2,3,5,6,20,21</sup> has concluded that that extension of refractoriness is the predominant mechanism by which the shock restores normal cardiac function. Tissue that remains longer in refractory, i.e. inexcitable, state cannot be re-excited by an incoming wavefront. Thus, the incoming wavefronts die out since they have nowhere to go. Since defibrillation hypotheses have postulated that each cell becomes depolarized by the shock<sup>28,29</sup>, then extension of refractoriness appears to be a phenomenon on a cellular level<sup>1,2,20,21,30</sup>.

The first part of this simulation study thus examines the responses of single refractory cells to defibrillation shocks delivered at various intervals from the onset of the cellular action potential. Of particular interest is the extension of refractoriness following a strong defibrillation shock since it has clinical relevance. This study is the first to offer such results; they are the outcome of the development of our computational tools that make possible the examination of cell and tissue behavior under strong electric fields. Although single cell behavior as observed here is consistent with previous modeling and experimental research<sup>20,21,30</sup>, it offers a limited understanding of the electrical processes that take place during and after the defibrillation shock. The reason for this is that the behavior of interconnected cells is far more complicated. It involves phenomena not observed on the cellular level such as, for instance, the formation of adjacent regions of depolarization and hyperpolarization (virtual cathodes and anodes) following a cathodal (depolarizing) stimulus<sup>11</sup>. Our results on the tissue level confirm this: although extension of refractoriness similar to the one demonstrated in cells subjected to strong or weak depolarizing stimuli (Fig. 1 panels (c) and (d)) is observed under the virtual cathodes (Figs. 3 and 4), the outcome of the shock depends on the global behavior of the tissue. The timing of the incoming wavefronts, both pre-existent and shock-induced, determines whether they will invade the central portion of the tissue. Indeed, Fig. 5 demonstrates that due to a lack of new excitation at the top right corner

of the tissue, the spiral wave has an excitable area in front of it allowing it to continue its propagation. Thus, extension of refractoriness, although very important mechanism for defibrillation, does not provide a complete description of the defibrillation process. The formation of new wavefronts at the break of the shock is an additional factor, the role of which needs to be fully elucidated in the future.

The present study is a step forward in the quest for uncovering the mechanisms of cardiac defibrillation. The major limitation of this study is the two-dimensional nature of the preparation. Although it incorporates (non-uniform) fiber curvature, shown by us to be of paramount importance to the generation of virtual electrodes throughout the tissue<sup>25,26,27</sup>, the geometry of the preparation is far from realistic. Nonetheless, we expect that when our computational capabilities allow us to examine the effect of the shock on the whole heart, we will obtain results consistent with the conclusions made in this study. The reason for this is that the shock-induced pattern of transmembrane potential, as obtained from passive models<sup>31</sup> is characterized with large-scale regions of depolarization and hyperpolarization in immediate proximity of each other. Thus, we expect that similar line of events will take place following a defibrillation shock in real hearts.

In this article we do not present a detailed simulation study examining all parameters that might have an impact on the success or failure of the shock. Rather, we focus on testing the role of the extension of refractoriness in defibrillation for a fixed set of parameters, such as tissue size, waveform shape and duration, and timing of the shock. The most clinically relevant of these parameters is the shape of the defibrillation pulse since biphasic shocks have been shown to defibrillate with less energy and voltage than monophasic<sup>32,33,34</sup>. The examination of the impact of these parameters, and most importantly, the shape of the shock waveform on the outcome of the shock is the focus of our forthcoming research.

### **Acknowledgments**

This research is supported by funds from contract LEQSF(1998-01)-RD-A-30 from the Louisiana Board of Regents through the Board of Regents Support Fund, and by NSF GIG Award DMF-9709754.

## References

1. S. M. Dillon, *Circ. Res.* **69**, 842 (1991).
2. S. M. Dillon, *Circulation* **85**, 1865 (1992).
3. R. J. Sweeney *et al.*, *Circulation* **83**, 2057 (1991).
4. I. R. Efimov *et al.*, *J. Cardiovasc. Electrophysiol.* **8**, 1031 (1997).
5. S. Knisley *et al.*, *Am. J. Physiol.* **266**, H2348 (1994).
6. S. Knisley and B. Hill, *Circulation* **88**, 2402 (1993).
7. O. Tovar and J. Jones, *Am. J. Physiol.* **272**, H1011 (1997).
8. S. Knisley *et al.*, *Biophys. J.* **66**, 719 (1994).
9. S. Knisley, *Circ. Res.* **77**, 1229 (1995).
10. J. P. Wikswo Jr *et al.*, *Biophys. J.* **69**, 2195 (1995).
11. N. G. Sepulveda *et al.*, *Biophys. J.* **55**, 987 (1989).
12. N. A. Trayanova and T. Pilkington, in *High-performance computing in biomedical research*, T. Pilkington *et al.*, eds., 403–425 (CRC Press, Boca Raton, FL, 1993).
13. G. Beeler and H. Reuter, *J. Physiol.* **268**, 177 (1977).
14. J.-P. Drouhard and F. A. Roberge, *IEEE Trans. Biomed. Eng.* **29**, 494 (1982).
15. K. Skouibine *et al.*, *IEEE Trans. Biomed. Eng.* (in press).
16. C. S. Henriquez, *Crit. Rev. Biomed. Eng.* **21**, 1 (1993).
17. W. Krassowska, *PACE* **18**, 1644 (1995).
18. B. J. Roth, *IEEE Trans. Biomed. Eng.* **42**, 1174 (1995).
19. N. A. Trayanova *et al.*, *Progress Biophys & Mol Biol* (in press).
20. J. L. Jones *et al.*, *IEEE Trans. Biomed. Eng.* **41**, 60 (1994).
21. J. L. Jones and O. H. Tovar, *J. Electrocardiol.* **28(Suppl)**, 25 (1995).
22. M. G. Fishler *et al.*, *J. Electrocardiol.* **28(Suppl)**, 174 (1995).
23. M. G. Fishler *et al.*, *Biophys. J.* **70**, 1347 (1996).
24. O. H. Tovar and J. L. Jones, *Circ. Res.* **77**, 430 (1995).
25. N. A. Trayanova *et al.*, *IEEE Trans. Biomed. Eng.* **40**, 899 (1993).
26. N. A. Trayanova *et al.*, *Chaos* **8**, 221 (1998).
27. E. Entcheva *et al.*, *IEEE Trans. Biomed. Eng.* (in press).
28. R. Plonsey and R. Barr, *Med. & Biol. Eng. & Comput.* **24**, 137 (1986).
29. W. Krassowska *et al.*, *IEEE Trans. Biomed. Eng.* **34**, 555 (1987).
30. J. L. Jones, in *Defibrillation of the heart*, W. A. Tacker, ed., chap. 3, 46–81 (Mosby Year Book, St. Louis, MO, 1994).
31. N. A. Trayanova and J. Eason, *PACE* **17**, 331 (1995).
32. E. G. Dixon *et al.*, *Circulation* **76**, 1176 (1987).
33. S. Saskena *et al.*, *Am. J. Cardiol.* **70**, 304 (1992).
34. J. Jones *et al.*, *Am. J. Physiol.* **253**, H1418 (1987).